ACS APPLIED MATERIALS & INTERFACES

www.acsami.org

Research Article

Thermal Interface Materials with High Thermal Conductivity and Low Young's Modulus Using a Solid−Liquid Metal Codoping Strategy

Xu-Dong Zhang, Zi-Tong Zhang, Hong-Zhang Wang, and Bing-Yang Cao*

Cite This: *ACS Appl. Mater. Interfaces* 2023, 15, 3534−3542

Read Online

ACCESS | Metrics & More | Article Recommendations | Supporting Information

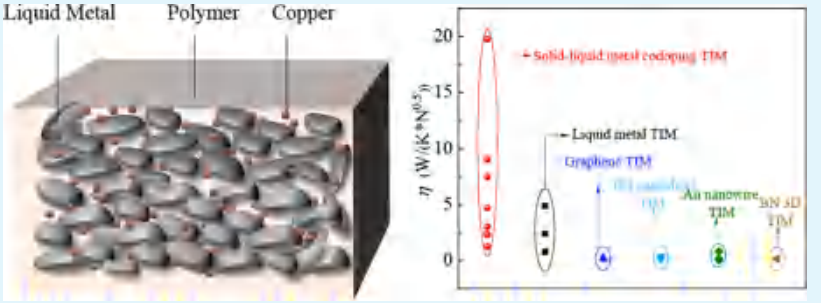

ABSTRACT: Thermal interface materials (TIMs), as typical thermal functional materials, are highly required to possess both high thermal conductivity and low Young's modulus. However, the naturally synchronized change in the thermal and mechanical properties seriously hinders the development of high-performance TIMs. To tackle such a dilemma, a strategy of codoping solid fillers and liquid metal fillers into polymer substrates is proposed in this study. This strategy includes a large amount of liquid metals that play the role of thermal paths and a small amount of uniformly dispersed solid fillers that further enhance heat conduction. Through the synergistic effect of the liquid metal and solid fillers, the thermal conductivity can be improved, and Young's modulus can be kept small simultaneously. A typical TIM with a volume of 55% gallium-based liquid metal and 15% copper particles as fillers has a thermal conductivity of 3.94 W/(m·K) and a Young's modulus of 699 kPa, which had the maximum thermomechanical performance coefficient compared with liquid metal TIMs and solid filler-doped TIMs. In addition, the thermal conductivity of the solid−liquid metal codoped TIM increased sharply with an increase of liquid metal content, and Young's modulus increased rapidly with an increase of the volume ratio of copper and polymer. The high−low-temperature cycling test and large-size light-emitting diode (LED) application demonstrated that this TIM had stable physical performance. The synergistic effect of the solid fillers and liquid metal fillers provides a broad space to solve the classic tradeoff issue of the mechanical and thermal properties of composites.

KEYWORDS: *thermal interface material, thermal conductivity, Young's modulus, solid−liquid metal codoping, thermomechanical performance coefficient*

1. INTRODUCTION

Thermal interface materials (TIMs) are indispensable functional materials for the thermal management of high heat flux devices,[1,2] such as electronic chips, high-energy lasers, and radars, that act by filling the contact surfaces between electronic devices and radiators. An ideal TIM should have high thermal conductivity and low Young's modulus.[3] However, high thermal conductivity and low Young's modulus of materials are naturally a pair of contradictions.[4] It can be verified from the fact that diamond,[5] carbon nanotubes,[6] and graphene[7] have high thermal conductivities and high hardness simultaneously, while polymers have low thermal conductivities and low hardness simultaneously. The synchronized change in the two physical properties seriously hinders the development of high-performance TIMs.

Thermal interface materials are typically made up of polymers and highly thermally conductive fillers, such as metal powders,[8,9] metallic oxides,[10] BN,[11] AlN,[12] and carbon materials.[13,14] According to the classical M−G model,[15] the thermal conductivity of a TIM exponentially increases with an increase of doping volume. In addition, according to Eshelby's theory,[16] Young's modulus will also sharply increase with an increase of solid filler content. The synchronized increase of the two physical properties will result in the dilemma of low thermal

Received: November 21, 2022
Accepted: December 26, 2022
Published: January 5, 2023

https://doi.org/10.1021/acsami.2c20713
ACS Appl. Mater. Interfaces 2023, 15, 3534−3542

conductivity at a small doping volume and high hardness at a large doping volume. Akhtar[17] predicted that the thermal conductivity of the Al_2O_3–epoxy composite would increase from 0.18 to 2.37 W/(m·K), and the tensile modulus would increase from 1.3 to 5.3 GPa with an increase in doping volume fraction of Al_2O_3 from 0 to 60%. Constructing a thermal path inside the composite is an effective method to improve the thermal conductivity under a small doping percentage, and this can be achieved using the freeze-drying method,[18] the template method,[19] the in situ growth method,[20] and other techniques.[21] Although the doping volume fraction was small by the above methods, the continuous mechanical structure sharply increased the Young's modulus of the composite, and it even reached GPa.[22] In addition, increasing the bonding force between solid fillers and polymers can also improve the thermal conductivity of a composite by enhancing the interfacial transport of phonons.[23,24] However, a firm interface structure significantly reduces the flexibility of composites.

Liquid metal is a novel type of thermal conductive filler[25−28] that possesses a series of excellent properties beyond solid fillers, including low Young's modulus (far less than that of a polymer), good dispersion (the droplet diameter of the ultrasonic crushing is less than 20 nm), and high allowable doping percentage. Young's modulus of composites doped with 10 μm copper particles and 10 and 100 μm liquid metal were compared (Figure 1), and the detailed calculation process[29,30] can be found in

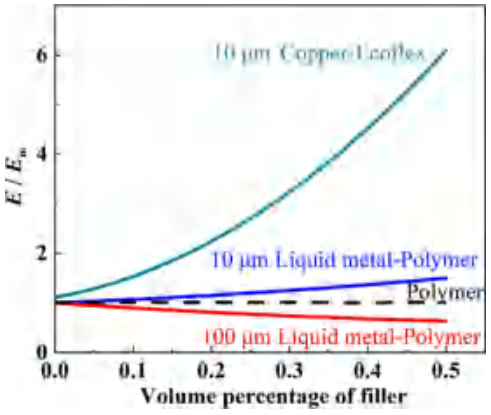

Figure 1. Young's modulus, E, of the composite varying with the volume percentage of the fillers, in which Ecoflex was embedded with 10 μm spherical copper particles and 10 and 100 μm liquid metal droplets, and Young's modulus, E_m, of the polymer.

Figure S1 and Tables S1−S3. It can be seen that Young's modulus of the liquid metal–polymer gradually decreased or slightly increased with an increase of liquid metal filler content, while that of the copper–polymer sharply increased with an increase of copper filler content. In most past research studies, the size of liquid metal was usually lower than 10 μm and even tens of nanometers. However, we first numerically disclosed that Young's modulus of composites is inversely proportional to the size of liquid metal droplets. This indicated that a composite with a low Young's modulus can be prepared by a liquid metal filler. However, it should be noted that the thermal conductivity of the liquid metal (20−40 W/(m·K))[31,32] is far lower than that of copper (398 W/(m·K)). In the work of Mei et al.,[33] the thermal conductivity of the liquid metal composite was only 1.0 W/(m·K) when the doping amount was 40%. Therefore, for solid filler doping, high thermal conductivity can be obtained, but the composite would be too hard. For liquid metal doping, a low Young's modulus can be obtained, but the thermal conductivity would be low. Hence, the thermal–mechanical tradeoff relationship remains a challenge for TIMs when embedding matrices with solid fillers and liquid metals, respectively.

To tackle this dilemma, a strategy of codoping solid fillers and liquid metal fillers into matrices, in which a large amount of liquid metal plays the role of a thermal path and a small amount of uniformly dispersed solid filler can further enhance heat conduction, is proposed in this study. Because the doping volume of the solid filler is small, Young's modulus will only slightly increase. Due to the synergistic effect of the liquid metal and the solid filler, the thermal conductivity can be improved, and Young's modulus can be kept small. In this study, a gallium–indium alloy is used as the liquid metal filler, copper as the solid filler, and Ecoflex as the polymer. The TIM with 55% gallium-based liquid metal and 15% copper as fillers had a thermal conductivity of 3.94 W/(m·K) and Young's modulus of 699 kPa.

2. RESULTS AND DISCUSSION

2.1. Fabrication and Characterization. Some recent studies have reported several materials by introducing liquid metal and rigid fillers into a polymer.[34−36] However, the preparation method included first mixing liquid metal with metal powder. Liquid metal gallium can corrode with most of the metals, like copper, aluminum, and iron. To avoid corrosion, in this paper, the liquid metal was first mixed with a polymer, and copper was then mixed. Therefore, there is no direct contact between the liquid metal and copper. Figure 2a shows the preparation procedure of solid–liquid codoped TIM. According to a specific volume fraction, liquid metal $GaIn_{24.5}$ and Ecoflex were preweighed and poured into a glass beaker. The mixing process was then conducted using an electric mixer in air for 30 min. During the stirring process, a small amount of the liquid metal was oxidized, resulting in a decrease of surface tension of the liquid metal, which was conducive to mixing the liquid metal with Ecoflex. Then, copper fillers with average diameters of 2 μm (Figure 2b) were poured into the mixture and stirred for 30 min. Finally, the three-phase slurry was heated to cure for 2 h at 70 °C. The real copper–liquid metal codoped TIM was red, consistent with the color of the copper particles.

Figure 2c,d shows the schematic diagram and the optical morphology of the copper–liquid metal codoped TIM. In fact, under the action of long-time stirring, the liquid metal will convert from a spherical shape to an irregular shape. This is because the solid gallium oxide coating on the surface of gallium prevents the transition of liquid gallium to the spherical shape. It can be seen that the liquid metal filler constructed a thermal network in Ecoflex, and the sizes of the liquid metal droplets were on the order of 100 μm, which was conducive to obtaining a small Young modulus than that of 10 μm, according to Figure 1. Figure 2e,f shows the scanning electron microscopy (SEM) image and atom distribution. It can be seen that the copper powder was uniformly dispersed in Ecoflex but not in the liquid metal. Because the Young's modulus of the liquid metal was much smaller than that of the polymer, the liquid metal thermal path did not increase the Young's modulus of the TIM. In addition, a small amount of copper filler will only slightly increase the Young's modulus. The microstructure of TIM under different magnifications can be seen in Video S1.

The solid–liquid codoped TIM exhibited good flexibility (Figure 3a), compressibility (Figure 3b), and stretchability

https://doi.org/10.1021/acsami.2c20713
ACS Appl. Mater. Interfaces 2023, 15, 3534−3542

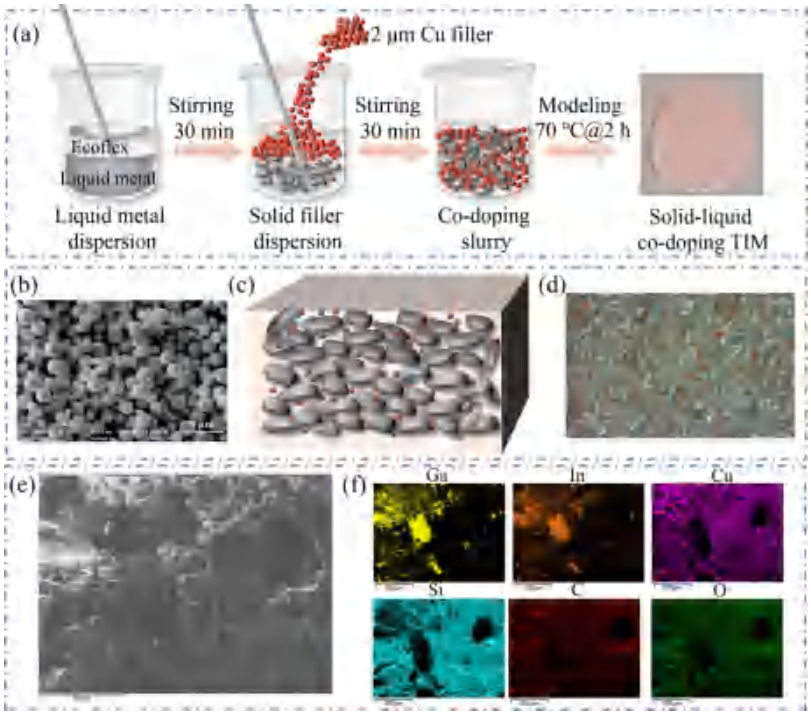

Figure 2. (a) Preparation procedure of the solid−liquid codoped thermal interface material, (b) sizes of the copper particles, (c) schematic diagram, (d) optical morphology, (e) SEM image, and (f) atom distribution.

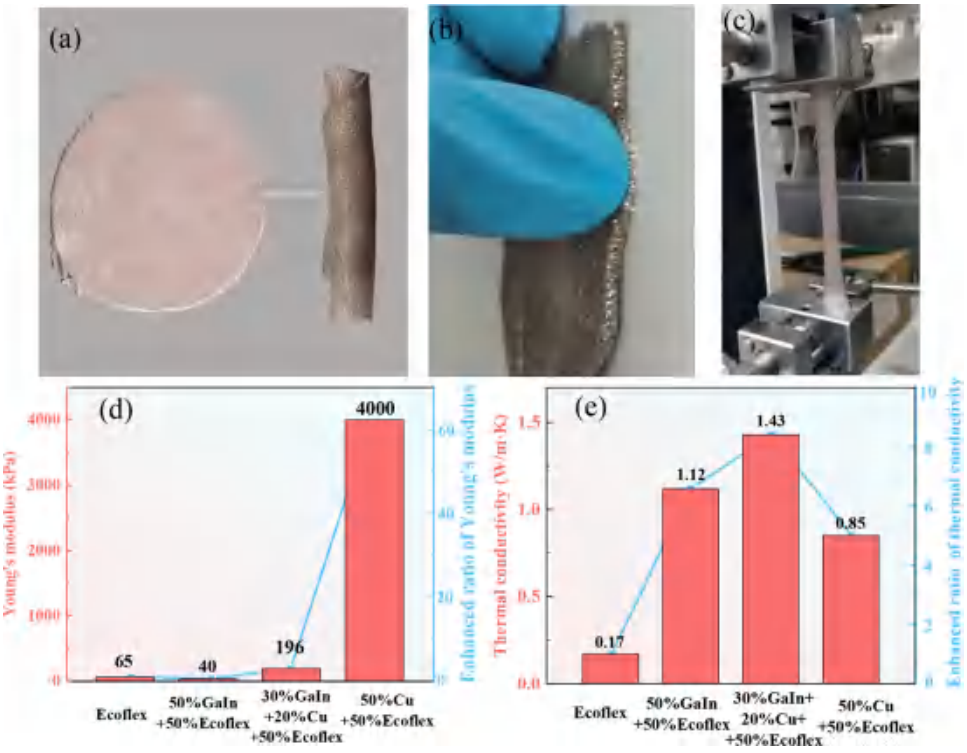

Figure 3. (a) Flexibility, (b) compressibility, (c) stretchability, and (d) Young's moduli, and (e) thermal conductivities of the TIMs with different fillers with a filling volume of 50%.

(Figure 3c). Figure 3d,e shows the comparison of the Young's modulus and thermal conductivities of the four types of TIMs: Ecoflex itself, the liquid metal (50%) TIM, the liquid metal (30%)−Cu (20%) TIM, and the copper (50%) TIM. It can be seen that the liquid metal (30%)−Cu (20%) TIM had the largest thermal conductivity, which was ∼8 times greater than that of Ecoflex itself, and the Young modulus of the liquid metal (30%)−Cu (20%) TIM (196 kPa) was similar to that of Ecoflex (65 kPa), which was much less than that of the Cu (50%) TIM (4000 kPa). It is worth mentioning that although the thermal conductivity of copper was larger than that of the liquid metal, it was difficult to disperse a high volume fraction of solid copper

https://doi.org/10.1021/acsami.2c20713
ACS Appl. Mater. Interfaces 2023, 15, 3534−3542

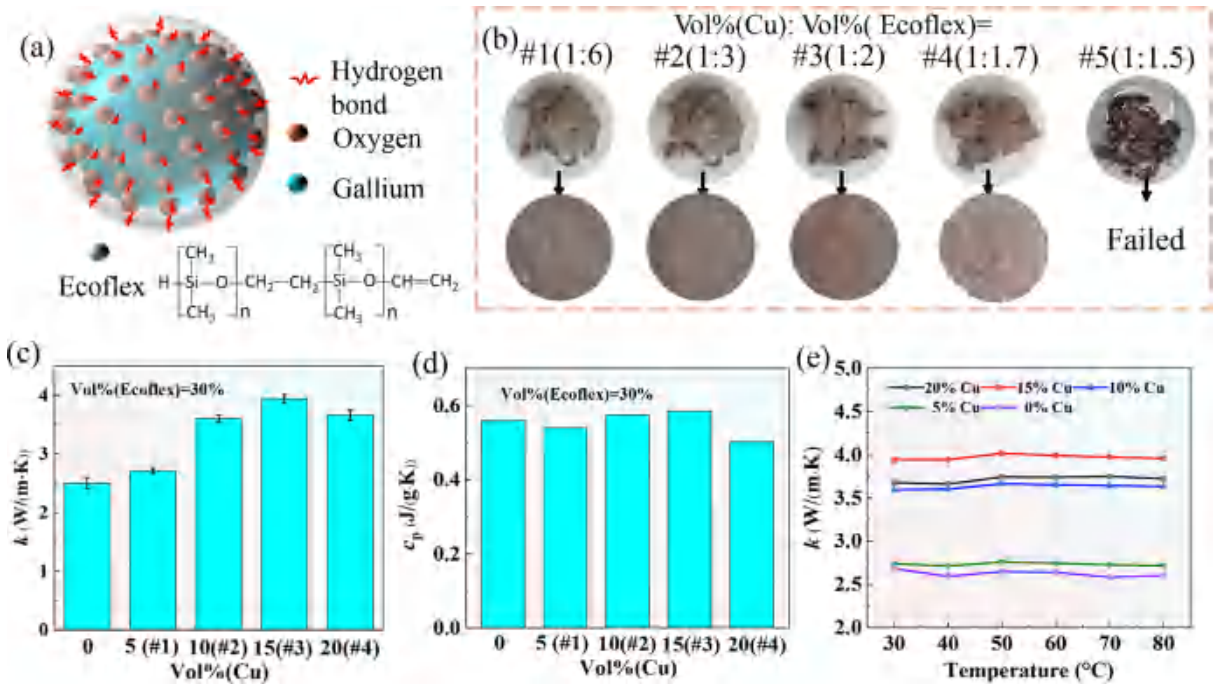

Figure 4. (a) Dispersion mechanism of the liquid metal in Ecoflex, (b) codoping the slurry with different volume ratios of copper powder and Ecoflex, (c) variation of thermal conductivities with the volume percentages of copper powder, (d) variation of heat capacities with volume percentages of copper powder, and (e) variation of thermal conductivities with temperature.

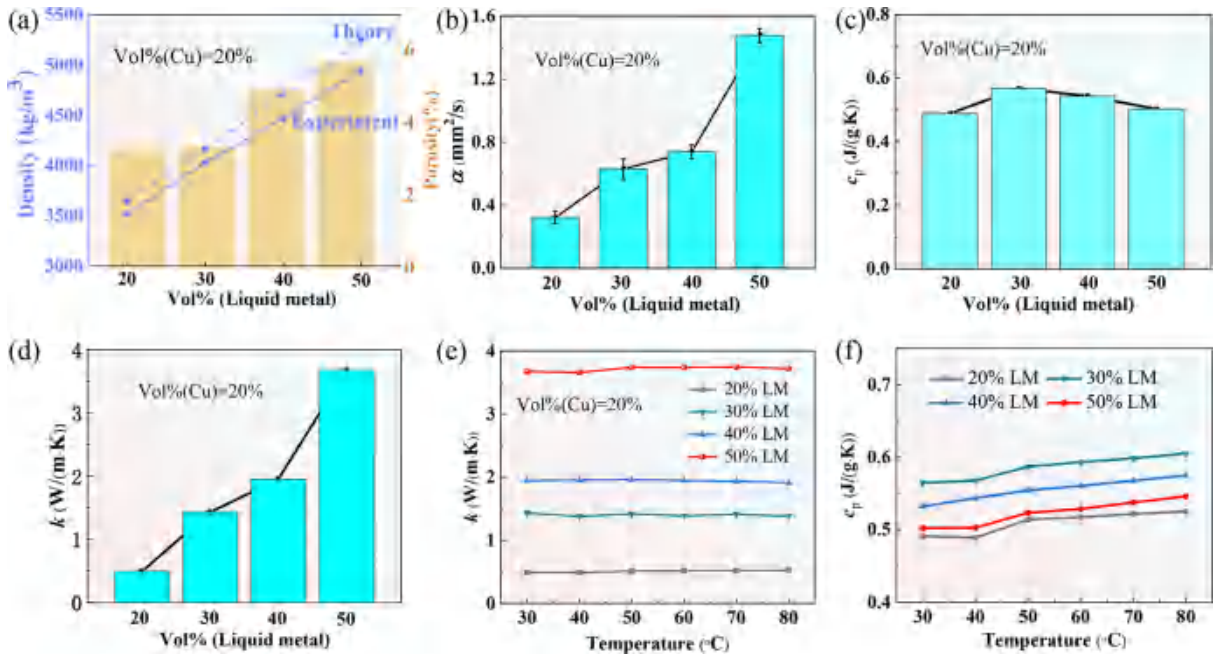

Figure 5. (a) Density and porosity, (b) thermal diffusivity, (c) heat capacity, (d) thermal conductivity, (e) variation of thermal conductivity with temperature, and (f) variation of heat capacity with temperature.

powder into Ecoflex, resulting in low thermal conductivity of the copper (50%) TIM (0.85 W/(m·K)). The comparison verified that the solid–liquid codoped TIM had better thermal and mechanical properties than the liquid metal TIM and copper TIM.

2.2. Thermal and Mechanical Performance. During the continuous stirring process, gallium chemically oxidizes and gallium oxide can form a hydrogen bond with Ecoflex.[37,38] Such an interaction force between the liquid metal and Ecoflex led to a stable structure to prevent the agglomeration of the liquid metal (Figure 4a). The oxidation and fluidity of the liquid metal enabled good dispersion of the liquid metal in Ecoflex. However, the addition of copper powder squeezed the doping space of the liquid metal and thus significantly reduced the doping amount of the liquid metal. It can be seen from Figure 4b that as the volume fraction of the copper powder increased, the codoping slurry became stickier and harder. When the volume ratio of the copper and Ecoflex was 1:1.5, the liquid metal was extruded from the

https://doi.org/10.1021/acsami.2c20713
ACS Appl. Mater. Interfaces 2023, 15, 3534−3542

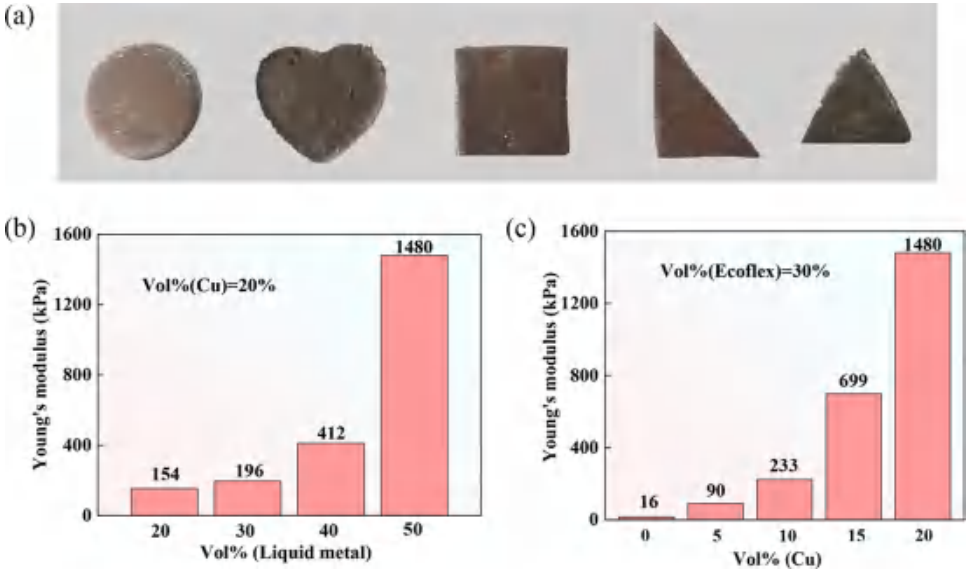

Figure 6. (a) Thermal interface materials of different shapes cut with scissors, (b) Young's modulus of the TIMs with the doping percentage of copper kept constant at 20%, and (c) Young's modulus of the TIMs with the volume percentage of Ecoflex kept constant at 30%.

slurry. Therefore, the maximum volume ratio of the copper and the Ecoflex was determined to be 1:1.7.

Figure 4c shows the thermal conductivities of the TIMs with different volume percentages of copper when maintaining the volume of the Ecoflex at 30%. In addition, the copper volumes of 5%, 10%, 15%, and 20% correspond to #1, #2, #3, and #4 TIMs in Figure 4b, respectively. This demonstrated that with an increase of copper volume percentage, the thermal conductivity of the solid−liquid codoped TIM first increased and then decreased. When the doping percentage of the copper powder was 15%, the thermal conductivity reached the maximum value of 3.94 W/(m·K). Figure 4d shows the heat capacity of five such TIMs. This figure demonstrates that the heat capacity almost remained constant when the volume of Ecoflex was 30%. This was because the heat capacity of the liquid metal (~400 J/(g·K))[39,40] was very close to that of copper (390 J/(g·K)). Even if the volume ratio of the two was changed, the total heat capacity changed little. Figure 4e shows the variation of thermal conductivity with temperature. It can be seen that the thermal conductivity changed little in the range of 30−80 °C.

While maintaining the volume percentage of copper at 20%, the solid−liquid codoped TIMs with different volume percentages of the liquid metal were prepared and tested. Figure 5a shows the densities and porosities of the TIMs. The densities of the TIMs nearly linearly increased with an increase of liquid metal percentage, and the porosity increased with a decrease in the volume percentage of Ecoflex. This was due to the high viscosity of the codoping slurry; hence, it was difficult to completely exhaust the air. The porosity was calculated using the density difference of the experimental density and the theoretical density, as shown in eq S2. Figure 5b,c shows the experimental data of the thermal diffusivity, α, and the heat capacity, c_p. It can be seen that the thermal diffusivity increased sharply with an increase of the liquid metal doping volume, and the heat capacity decreased with an increase of doping volume. The thermal conductivity was then calculated using the product of the density, heat capacity, and thermal diffusivity, as shown in Figure 5d. When the doping volume percentage of the solid−liquid filler was 70% (copper filler 20% + liquid metal filler 50%), the thermal conductivity reached 3.6 W/(m·K). The normal operating temperature range of electronic devices (30−80 °C) and the changes of the thermal conductivity and heat capacity of the TIMs were within 10% (Figure 5e,f). This result indicated that the thermal performances of the TIMs remained nearly stable over a wide temperature range.

The solid−liquid codoped TIM could be easily cut into customized shapes using scissors to meet the needs of various scenes, such as circles, heart-shaped, squares, and triangles (Figure 6a). Young's modulus of the TIM was measured when maintaining the volume percentage of the copper constant at 20% and the volume percentage of copper at 30%. It can be seen from Figure 6b that with an increase of liquid metal volume percentage, Young's modulus gradually increased. This was because the volume fraction of Ecoflex gradually decreased and the volume ratio of copper and Ecoflex increased. Hence, the hardness of the composite increased. It can be seen from Figure 6c that with an increase of copper volume fraction, Young's modulus increased. This demonstrated that Young's modulus of the solid−liquid codoped TIM was primarily determined by the volume ratio of copper and the polymer. According to the predicated results in Figure 1, Young's modulus of composites will sharply increase with an increase of volume percentage of copper while slightly increase or decrease with an increase of volume percentage of liquid metal. Therefore, the dominated factor affecting Young's modulus of the composite should be the volume percentage of copper but not liquid metal. The larger the volume ratio, the greater the Young modulus. When the doping percentage of the copper particles was 20%, the Young modulus of the TIM was as high as 1480 kPa.

Figure 7 shows the comparison of the thermal and mechanical properties of the solid−liquid codoped TIM and other TIMs. We selected the TIMs with Young's modulus of less than 25 MPa for comparison.[41−46] In this range, the doping volume percentage of the solid fillers was generally less than 5%. It can be seen that the TIMs doped with solid fillers generally had large Young's modulus, and the thermal conductivities were lower than 1.5 W/(m·K). The Au nanowire TIM[44] was an exception; it had a maximum thermal conductivity of 5.1 W/(m·K), and its Young's modulus (6 MPa) was far larger than that of the solid−liquid codoped TIM. The liquid metal TIM[46] had the minimum

https://doi.org/10.1021/acsami.2c20713
ACS Appl. Mater. Interfaces 2023, 15, 3534−3542

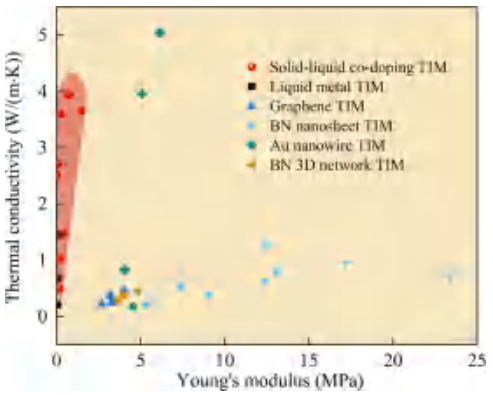

Figure 7. Comparison of the thermal conductivity and Young's modulus of the solid−liquid codoped TIM with those of the other TIMs.

Young's modulus, while its thermal conductivity was less than 1.5 W/(m·K). The solid−liquid codoped TIM in this study had the best thermomechanical performance; it also had the maximum thermal conductivity of 3.94 W/(m·K) with a Young's modulus of 699 kPa.

The approximate relationship between the thermal conductivity and Young's modulus for nonmetallic and electrically insulating solids was already derived before, and it is shown in eq 1.[47] In eq 1, k is the thermal conductivity of the material, E is the Young's modulus of the material, c_v is the heat capacity of the material, l is the mean free path of a phonon in the material, and ρ is the density of the material. This implies that the thermal conductivity will increase with the square root of the Young's modulus. Therefore, we defined a thermomechanical performance coefficient, η, to evaluate the comprehensive performance of different TIMs, as shown in eq 2. The greater the influence factor, η, the better the comprehensive thermal and mechanical performance of the TIM. Figure 8 shows the η's of different

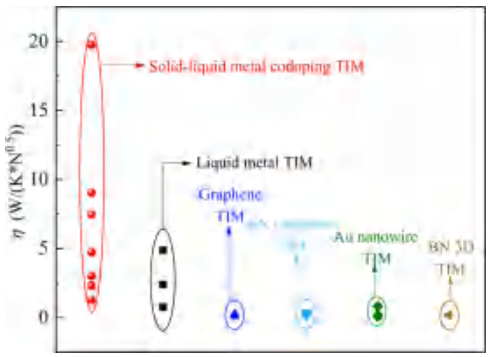

Figure 8. Thermomechanical influence factors, η, of different TIMs.

TIMs. It can be seen that solid−liquid metal codoped TIMs had the maximum η, followed by the liquid metal TIMs. In addition, the solid filler-doped TIMs had very small factors due to the large Young's modulus.

$$k \approx \frac{C_v l}{3}\cdot\left(\frac{E}{\rho}\right)^{1/2} \quad (1)$$

$$\eta = \frac{k}{E^{1/2}} \quad (2)$$

2.3. Long-Term Reliability. The thermal powers of electronic devices change dramatically due to the frequent switching on and off or working frequency adjustments. Therefore, the TIMs sandwiched between the heat source and the heat sink always withstand continuous high−low-temperature cycles, and this requires long-term reliability. Figure 9a shows a high−low-temperature testing platform with a working range from −10 to 200 °C. The heat source is the heating plate at the bottom, the heat sink is the air-cooled heat pipe radiator at the upper portion, and the TIM is sandwiched in the middle. The heat sink works continuously, and the heat source works intermittently with a cycle time of 12 min (4 min of operation and 8 min of shutdown). For real-time monitoring of temperature, a thermocouple was pasted below the TIM, and the temperature was varied from 55 to 35 °C (Figure 9b,c). A total of 200 cycles were conducted, and after every 50 cycles, the thermal conductivity and Young's modulus were measured. The tested TIM was made up of 5% Cu, 65% liquid metal, and 30% Ecoflex. It can be seen that the thermal conductivity and Young's modulus after 200 cycles did not notably change (Figure 9d,e). The high−low-temperature cycles indicated the excellent long-term reliability of the solid−liquid codoped TIM. In fact, the solid−liquid codoped TIM was already cured, and the internal filler distribution will not change with time. Hence, the thermal and mechanical properties will not change with time.

2.4. Applications. Due to the machining tolerance or uneven installation torque, large-sized devices will slightly warp when installed on a radiator, thus resulting in a large gap. In this situation, the thermal grease fails, and a thermal pad is typically used. The solid−liquid codoped TIM was compared with the thermal grease from Shintsu Corporation and a thermal pad from Liard Corporation. Figure 10a shows the experimental platform, in which a 50 W LED was selected as the heat source, and the radiator was the air-cooled straight-fin radiator. It can be seen that when the LED was directly mounted on the radiator, warping occurred at the boundary. Figure 10b shows the temperature cloud diagram of the LED when using no TIM, thermal grease, Liard thermal pad, and solid−liquid codoped TIM. With an increase in working time, the maximum temperature of the LED lamp gradually increased and finally reached stability. When the TIM was not used, the LED surface temperature reached 72 °C in 37 s, and the temperatures of the thermal grease, the Liard thermal pad, and the solid−liquid codoped TIM were 58.6, 50.8, and 51.3 °C, respectively. Figure 10c shows the temperature curves of the heating and cooling processes when using different TIMs. It can be seen that the solid−liquid codoped TIM showed a thermal performance equivalent to that of the Liard thermal pad, and both were better than that of the thermal grease. According to the thermal analysis presented in Table S4, compared with no TIM, the total thermal resistance when using the solid−liquid codoped TIM was reduced from 1.28 to 0.82 (°C·cm^2)/W. Moreover, the extrusion will irreversibly deform the thermal pad and thermal grease, which can only be used once. However, the solid−liquid codoped TIM can return to its original shape after the pressure is removed, which makes it reusable.

3. CONCLUSIONS

In this study, we demonstrated a solid−liquid metal codoped TIM with favorable thermal and mechanical properties that overcame the tradeoff relationship between high thermal conductivity and low Young's modulus. By utilizing a solid−liquid metal codoping strategy, the typical TIM achieved a

https://doi.org/10.1021/acsami.2c20713
ACS Appl. Mater. Interfaces 2023, 15, 3534−3542

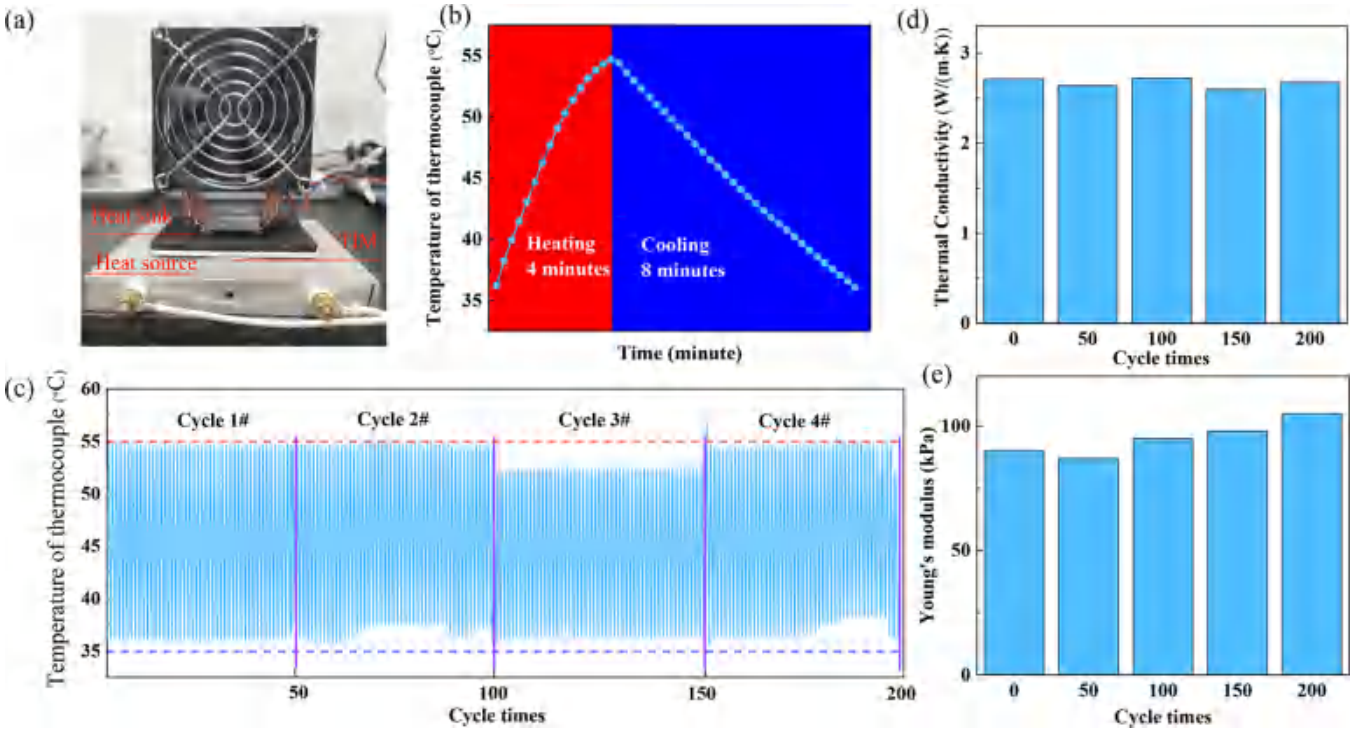

Figure 9. (a) Experimental platform, (b) temperature variation in one cycle, (c) temperature variation in 200 cycles, (d) variation of thermal conductivity with cycle times, (e) variation of Young's modulus with cycle times.

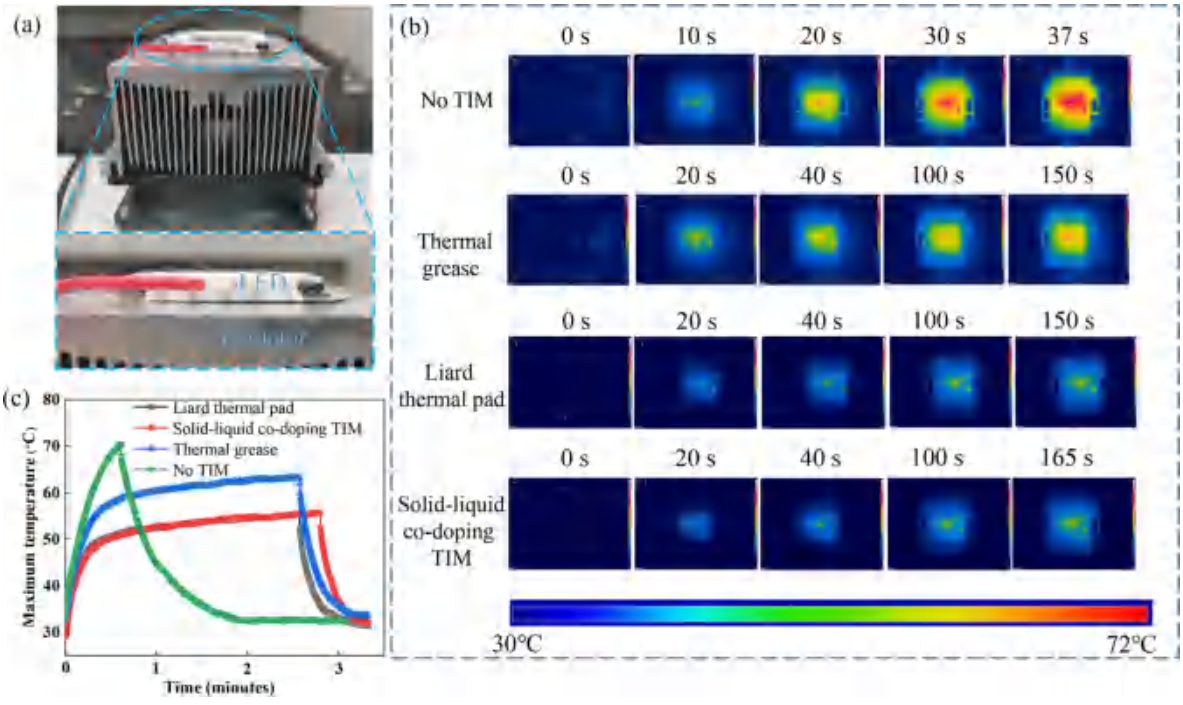

Figure 10. (a) Morphology of the LED and radiator, (b) temperature cloud diagram of the LED, and (c) maximum temperature curves of the LED.

thermal conductivity of 3.94 W/(m·K) and a Young modulus of 699 kPa, with 55% gallium-based liquid metal and 15% copper as fillers. The thermal conductivity of the TIM increased sharply with the doping volume percentage of the liquid metal, and the Young's modulus increased rapidly with the volume ratio of the copper and Ecoflex. The comprehensive performance was better than that of the liquid metal TIM and the solid filler-doped TIM. This TIM had the maximum thermomechanical performance coefficient compared with liquid metal TIMs and solid filler-doped TIMs. In addition, the TIM maintained a stable physical performance under 200 cycles of high−low-temperature tests. The large-sized LED application test showed that this TIM was suitable for filling gaps. In summary, the synergistic effect of the solid filler and liquid metal provided a broad space to solve the classic tradeoff of mechanical and thermal properties.

https://doi.org/10.1021/acsami.2c20713
ACS Appl. Mater. Interfaces 2023, 15, 3534−3542

4. EXPERIMENTAL SECTION

4.1. Materials. $GaIn_{24.5}$ was prepared as follows. Gallium and indium were weighed with mass percentages of 75.5 and 24.5%, respectively, and then, the mixture was heated using an induction furnace until it melted completely. The liquid metal was then cooled to 80 °C and stirred until uniformly mixed. Finally, the furnace was cooled to 25 °C, and $GaIn_{24.5}$ was obtained. Gallium and indium were purchased from Hunan Sinen Materials Co., Ltd., China. Copper was purchased from Qinghe Huiguang Metal Materials Co., Ltd., China. Ecoflex was purchased from Smooth-On, and its brand was Ecoflex-0030.

4.2. Thermal and Mechanical Property Tests. The density was obtained by dividing the mass by the volume of a cylindrical sheet TIM. The mass of the TIM was tested using an electronic balance (accuracy of 0.0001 g), and the volume of the TIM was obtained by measuring the diameter and height of the cylindrical sheet TIM, which was measured using a vernier caliper (accuracy of 0.02 mm). The thermal diffusivity was tested using the laser flash method (NETZSCH, LFA 467), and the heat capacity was tested using differential scanning calorimetry (NETZSCH, DSC3500). Young's modulus was tested using a universal testing machine (Dongguan Bolaide Equipment Co., Ltd., BLD-1028A). Infrared thermal imager Fotric 220s was from Fotric Inc., China.

4.3. High−Low-Temperature Cycle Test. A T-type thermocouple was used to monitor the temperature variation, and the signals were collected by an Agilent 34970 A with a sampling frequency of 4 times/min. The thermocouple was pasted on the contact surface of the heat sink and the TIM. The switch of the heat source was controlled by a time switch. After every 50 cycles, a knife was used to cut a small piece of the TIM for testing.

4.4. LED Applications. The warping between the LED and radiator was created deliberately. The two bolts on the left side of the LED were tightened, and the two bolts on the right side of the LED were slightly tightened. There was a gap of 80 μm on the right side of the LED due to different forces on both sides. An infrared imager was used to test the surface temperature of the LED; it was set to a timed automatic photo mode to monitor the temperature change during the continuous heating period.

■ ASSOCIATED CONTENT

Supporting Information

The Supporting Information is available free of charge at https://pubs.acs.org/doi/10.1021/acsami.2c20713.

Calculation of Young's modulus: composite doping with copper particles and liquid metal droplets, respectively, theoretical result of the liquid metal composite: porosity, thermal analysis, and total thermal resistance (PDF)

Microstructure of TIMs under different magnifications (Video S1) (MP4)

■ AUTHOR INFORMATION

Corresponding Author

Bing-Yang Cao − *Key Laboratory for Thermal Science and Power Engineering of Ministry of Education, Department of Engineering Mechanics, Tsinghua University, Beijing 100084, China*; orcid.org/0000-0003-3588-972X; Email: caoby@mail.tsinghua.edu.cn

Authors

Xu-Dong Zhang − *Key Laboratory for Thermal Science and Power Engineering of Ministry of Education, Department of Engineering Mechanics, Tsinghua University, Beijing 100084, China*

Zi-Tong Zhang − *Key Laboratory for Thermal Science and Power Engineering of Ministry of Education, Department of Engineering Mechanics, Tsinghua University, Beijing 100084, China*

Hong-Zhang Wang − *Department of Biomedical Engineering, School of Medicine, Tsinghua University, Beijing 100084, China*

Complete contact information is available at: https://pubs.acs.org/10.1021/acsami.2c20713

Notes

The authors declare no competing financial interest.

■ ACKNOWLEDGMENTS

This work was supported by the National Natural Science Foundation of China (Grant Nos. 51825601, 52206098, and U20A20301) and the China Postdoctoral Science Foundation (Grant No. 2021M701852).

■ REFERENCES

(1) Razeeb, K. M.; Dalton, E.; Cross, G. L. W.; Robinson, A. J. Present and Future Thermal Interface Materials for Electronic Devices. *Int. Mater. Rev.* **2018**, *63*, 1−21.

(2) Jasmee, S.; Omar, G.; Othaman, S. S. C.; Masripan, N. A.; Hamid, H. Interface Thermal Resistance and Thermal Conductivity of Polymer Composites at Different Types, Shapes, and Sizes of Fillers: A review. *Polym. Compos.* **2021**, *42*, 2629−2652.

(3) Chung, D. D. L. Performance of Thermal Interface Materials. *Small* **2022**, *18*, No. 2200693.

(4) Shen, S.; Henry, A.; Tong, J.; Zheng, R. T.; Chen, G. Polyethylene Nanofibers with Very High Thermal Conductivities. *Nat. Nanotechnol.* **2010**, *5*, 251−255.

(5) Olson, J. R.; Pohl, R. O.; Vandersande, J. W.; Zoltan, A.; Anthony, T. R.; Banholzer, W. F. Thermal Conductivity of Diamond between 170 and 1200 K and the Isotope Effect. *Phys. Rev. B* **1993**, *47*, 14850.

(6) Fujii, M.; Zhang, X.; Xie, H.; Ago, H.; Takahashi, K.; Ikuta, T.; Abe, H.; Shimizu, T. Measuring the Thermal Conductivity of a Single Carbon Nanotube. *Phys. Rev. Lett.* **2005**, *95*, No. 065502.

(7) Balandin, A. A.; Ghosh, S.; Bao, W.; Calizo, I.; Teweldebrhan, D.; Miao, F.; Lau, C. N. Superior Thermal Conductivity of Single-Layer Graphene. *Nano Lett.* **2008**, *8*, 902−907.

(8) Xu, J.; Munari, A.; Dalton, E.; Mathewson, A.; Razeed, K. M. Silver Nanowire Array-Polymer Composite as Thermal Interface Material. *J. Appl. Phys.* **2009**, *106*, No. 124310.

(9) Han, Y.; Ruan, K.; Gu, J. Multifunctional Thermally Conductive Composite Films Based On Fungal Tree-Like Heterostructured Silver Nanowires@ Boron Nitride Nanosheets and Aramid Nanofibers. *Angew. Chem., Int. Ed.* **2022**, No. e202216093.

(10) Ouyang, Y.; Bai, L.; Tian, H.; Li, X.; Yuan, F. Recent Progress of Thermal Conductive Polymer Composites: Al_2O_3 Fillers, Properties and Applications. *Composites, Part A* **2022**, *152*, No. 106685.

(11) Wang, D.; Ren, S.; Chen, J.; Li, Y.; Wang, Z.; Xu, J.; Jia, X.; Fu, J. Healable, Highly Thermal Conductive, Flexible Polymer Composite with Excellent Mechanical Properties and Multiple Functionalities. *Chem. Eng. J.* **2022**, *430*, No. 133163.

(12) Yu, H.; Li, L.; Kido, T.; Xi, G.; Xu, G.; Guo, F. Thermal and Insulating Properties of Epoxy/Aluminum Nitride Composites Used for Thermal Interface Material. *J. Appl. Polym. Sci.* **2012**, *124*, 669−677.

(13) Khan, J.; Momin, S. A.; Mariatti, M. A Review on Advanced Carbon-Based Thermal Interface Materials for Electronic Devices. *Carbon* **2020**, *168*, 65−112.

(14) Ruan, K.; Gu, J. Ordered Alignment of Liquid Crystalline Graphene Fluoride for Significantly Enhancing Thermal Conductivities of Liquid Crystalline Polyimide Composite Films. *Macromolecules* **2022**, *55*, 4134−4145.

(15) Xu, Y.; Wang, X.; Hao, Q. A Mini Review on Thermally Conductive Polymers and Polymer-Based Composites. *Compos. Commun.* **2021**, *24*, No. 100617.

(16) Vaitheeswaran, P. K.; Subbarayan, G. Estimation of Effective Thermal and Mechanical Properties of Particulate Thermal Interface Materials by a Random Network Model. *J. Electron. Packag.* **2018**, *140*, No. 020901.
(17) Akhtar, S. S. An Integrated Approach to Design and Develop High-Performance Polymer-Composite Thermal Interface Material. *Polymers* **2021**, *13*, 807.
(18) Bhanushali, S.; Ghosh, P. C.; Simon, G. P.; Cheng, W. Copper Nanowire-Filled Soft Elastomer Composites for Applications as Thermal Interface Materials. *Adv. Mater. Interfaces* **2017**, *4*, No. 1700387.
(19) Tian, Z.; Sun, J.; Wang, S.; Zeng, X.; Zhou, S.; Bai, S.; Zhao, N.; Wong, C. P. A Thermal Interface Material Based on Foam-Templated Three-Dimensional Hierarchical Porous Boron Nitride. *J. Mater. Chem. A* **2018**, *6*, 17540−17547.
(20) Xu, S.; Wang, S.; Chen, Z.; Sun, Y.; Gao, Z.; Zhang, H.; Zhang, J. Electric-Field-Assisted Growth of Vertical Graphene Arrays and the Application in Thermal Interface Materials. *Adv. Funct. Mater.* **2020**, *30*, No. 2003302.
(21) Huang, Z.; Wu, W.; Drummer, D.; Liu, C.; Wang, Y.; Wang, Z. Multi-Contact Hybrid Thermal Conductive Filler Al_2O_3@ AgNPs Optimized Three-Dimensional Thermal Network for Flexible Thermal Interface Materials. *J. Appl. Polym. Sci.* **2021**, *138*, 50889.
(22) Xu, Z.; Lin, G.; Sui, G. The Synergistic Effects on Enhancing Thermal Conductivity and Mechanical Strength of hBN/CF/PE Composite. *J. Appl. Polym. Sci.* **2020**, *137*, 49212.
(23) Kim, G. H.; Lee, D.; Shanker, A.; Shao, L.; Kwon, M. S.; Gidley, D.; Kim, J.; Pipe, K. High Thermal Conductivity in Amorphous Polymer Blends by Engineered Interchain Interactions. *Nat. Mater.* **2015**, *14*, 295−300.
(24) Zhang, X. D.; Yang, G.; Cao, B. Y. Bonding-Enhanced Interfacial Thermal Transport: Mechanisms, Materials, And Applications. *Adv. Mater. Interfaces* **2022**, *9*, No. 2200078.
(25) Kazem, N.; Hellebrekers, T.; Majidi, C. Soft Multifunctional Composites and Emulsions with Liquid Metals. *Adv. Mater.* **2017**, *29*, No. 1605985.
(26) Chen, S.; Wang, H. Z.; Zhao, R. Q.; Rao, W.; Liu, J. Liquid Metal Composites. *Matter* **2020**, *2*, 1446−1480.
(27) Wang, C.; Gong, Y.; Cunning, B. V.; Lee, S.; Le, Q.; Joshi, S.; Buyukcakir, O.; Zhang, H.; Seong, W. K.; Huang, M.; Wang, M.; Wang, M.; Lee, J.; Lee, J.; Kim, G.; Kim, G. H.; Ruoff, E. A General Approach to Composites Containing Nonmetallic Fillers and Liquid Gallium. *Sci. Adv.* **2021**, *7*, No. eabe3767.
(28) Yan, J.; Malakooti, M. H.; Lu, Z.; Wang, Z.; Kazem, N.; Pan, C.; Bockstaller, M.; Majidi, C.; Matyjaszewski, K. Solution Processable Liquid Metal Nanodroplets by Surface-Initiated Atom Transfer Radical Polymerization. *Nat. Nanotechnol.* **2019**, *14*, 684−690.
(29) Style, R. W.; Boltyanskiy, R.; Allen, B.; Jensen, K. E.; Foote, H.; Wettlaufer, J.; Dufresne, E. Stiffening Solids With Liquid Inclusions. *Nat. Phys.* **2015**, *11*, 82−87.
(30) Chiew, C.; Malakooti, M. H. A Double Inclusion Model for Liquid Metal Polymer Composites. *Compos. Sci. Technol.* **2021**, *208*, No. 108752.
(31) Zhang, X. D.; Sun, Y.; Chen, S.; Liu, J. Unconventional Hydrodynamics of Hybrid Fluid Made of Liquid Metals and Aqueous Solution under Applied Fields. *Front. Energy* **2018**, *12*, 276−296.
(32) Zhang, X. D.; Li, X. P.; Zhou, Y. X.; Yang, J.; Liu, J. Vascularized Liquid Metal Cooling for Thermal Management of KW High Power Laser Diode Array. *Appl. Therm. Eng.* **2019**, *162*, No. 114212.
(33) Mei, S.; Gao, Y.; Deng, Z.; Liu, J. Thermally Conductive and Highly Electrically Resistive Grease through Homogeneously Dispersing Liquid Metal Droplets inside Methyl Silicone Oil. *J. Electron. Packag.* **2014**, *136*, No. 011009.
(34) Tutika, R.; Zhou, S. H.; Napolitano, R. E.; Bartlett, M. D. Mechanical and Functional Tradeoffs in Multiphase Liquid Metal, Solid Particle Soft Composites. *Adv. Funct. Mater.* **2018**, *28*, No. 1804336.
(35) Guo, C.; Li, Y.; Xu, J. H.; Zhang, Q.; Wu, K.; Fu, Q. A Thermally Conductive Interface Material with Tremendous and Reversible Surface Adhesion Promises Durable Cross-Interface Heat Conduction. *Mater. Horiz.* **2022**, *9*, 1690−1699.
(36) Chen, S.; Xing, W.; Wang, H.; Cheng, W.; Lei, Z.; Zheng, F.; Tao, P.; Shang, W.; Fu, B.; Song, C.; Dickey, M. D.; Deng, T. A Bottom-Up Approach to Generate Isotropic Liquid Metal Network in Polymer-Enabled 3D Thermal Management. *Chem. Eng. J.* **2022**, *439*, No. 135674.
(37) Wang, D.; Wang, X.; Rao, W. Precise Regulation of Ga-Based Liquid Metal Oxidation. *Acc. Mater. Res.* **2021**, *2*, 1093−1103.
(38) Liu, Z.; Li, S.; Lin, S.; Shi, Y.; Yang, P.; Chen, X.; Wang, Z. L. Crystallization-Induced Shift in a Triboelectric Series and Even Polarity Reversal for Elastic Triboelectric Materials. *Nano Lett.* **2022**, *22*, 4074−4082.
(39) Zhang, X. D.; Yang, X. H.; Zhou, Y. X.; Rao, W.; Gao, J. Y.; Ding, Y. J.; Shu, Q. Q.; Liu, J. Experimental Investigation of Galinstan Based Minichannel Cooling for High Heat Flux and Large Heat Power Thermal Management. *Energy Convers. Manage.* **2019**, *185*, 248−258.
(40) Yang, X. H.; Liu, J.Advances in Liquid Metal Science and Technology in Chip Cooling and Thermal Management. In *Advances in Heat Transfer*; Elsevier, 2018; Vol. *50*, pp 187−300.
(41) Liu, Z.; Li, J.; Liu, X. Novel Functionalized BN Nanosheets/Epoxy Composites with Advanced Thermal Conductivity and Mechanical Properties. *ACS Appl. Mater. Interfaces* **2020**, *12*, 6503−6515.
(42) Jiang, F.; Song, N.; Ouyang, R.; Ding, P. Wall Density-Controlled Thermal Conductive and Mechanical Properties of Three-Dimensional Vertically Aligned Boron Nitride Network-Based Polymeric Composites. *ACS Appl. Mater. Interfaces* **2021**, *13*, 7556−7566.
(43) Wang, F.; Drzal, L. T.; Qin, Y.; Huang, Z. Mechanical Properties and Thermal Conductivity of Graphene Nanoplatelet/Epoxy Composites. *J. Mater. Sci.* **2015**, *50*, 1082−1093.
(44) Balachander, N.; Seshadri, I.; Mehta, R. J.; Schadler, L. S.; Tascius, T. B.; Keblinshi, P.; Ramanath, G. Nanowire-Filled Polymer Composites with Ultrahigh Thermal Conductivity. *Appl. Phys. Lett.* **2013**, *102*, No. 093117.
(45) Jeong, S. H.; Chen, S.; Huo, J.; Gamstedt, E. K.; Liu, J.; Zhang, S. L.; Zhang, Z. B.; Hjort, K.; Wu, Z. Mechanically Stretchable and Electrically Insulating Thermal Elastomer Composite by Liquid Alloy Droplet Embedment. *Sci. Rep.* **2015**, *5*, No. 18257.
(46) Bartlett, M. D.; Kazem, N.; Powell-Palm, M. J.; Majidi, C.; et al. High Thermal Conductivity in Soft Elastomers with Elongated Liquid Metal Inclusions. *Proc. Natl. Acad. Sci. U.S.A.* **2017**, *114*, 2143−2148.
(47) Plawsky, J. L.*Transport Phenomena Fundamentals*; CRC Press: Boca Raton, FL, 2014.

https://doi.org/10.1021/acsami.2c20713
ACS Appl. Mater. Interfaces 2023, 15, 3534−3542